Non-invasive analyze of boron and lithium in 18th century Chinese porcelain enamel and glaze: A PIXE/PIGE study

Jacques Burlot, Philippe Colomban, Ludovic Bellot-Gurlet, Quentin Lemasson, Laurent Pichon

Journal of the European Ceramic Society 44 (2024) 116746

Contents lists available at ScienceDirect

Journal of the European Ceramic Society

journal homepage: www.elsevier.com/locate/jeurceramsoc

Non-invasive analyze of boron and lithium in 18th century Chinese porcelain enamel and glaze: A PIXE/PIGE study

Jacques Burlot [a], Philippe Colomban [a,*], Ludovic Bellot-Gurlet [a], Quentin Lemasson [b,c], Laurent Pichon [b,c]

[a] Sorbonne Université, CNRS, De la Molécule aux Nano-Objets: Réactivité, Interactions et Spectroscopies, MONARIS UMR8233, 4 Place Jussieu, Paris 75005, France
[b] Ministère de la Culture, Centre de Recherche et de Restauration des Musées de France, Palais du Louvre, 14 quai François Mitterrand, Paris 75001, France
[c] Ministère de la Culture, CNRS, Lab-BC UAR 3506, Centre de Recherche et de Restauration des Musées de France, Palais du Louvre, 14 quai François Mitterrand, Paris 75001, France

ARTICLE INFO

Keywords:
Lithium
Boron
Enamels
Europe
China

ABSTRACT

In enamelling technology, the natural (raw) materials used before the middle of the 19th century combine by nature different elements whose role in the process can be important even in small quantities. Some of these elements – particularly boron, lithium – are difficult to measure non-invasively and are therefore rarely analyzed. Boron and lithium, often used as additional flux in glazes, were quantified by PIXE and PIGE analysis with the extracted beam of the New AGLAE facility in 18th century porcelains samples, French soft-paste from the Manufacture royale de Sèvres and Chinese hard-paste from the reign of the Qing dynasty. The results were compared to previous conclusions made using SEM/EDS and pXRF in order to assert the presence of boron, previously suspected by Raman microspectroscopy, and to detect the presence of lithium, both provided by a particular flux (borax), mentioned in the historical French and Chinese enamel recipes.

1. Introduction

Enamelled decoration is the most technically and aesthetically sophisticated part of many objects prepared by firing. The analysis of this decoration allows studying the history of production techniques, the transfers of know-how and tastes between production areas, thus helping to authenticate objects (originals, copies or fakes) or to date them. For decades, attention has been paid to the exchange of ceramic objects and associated technologies between Asia and Europe. We know indeed that the "*porcelain disease*" in the 17th and 18th centuries led to the importation of Chinese and Japanese porcelain into Europe and to the creation of European porcelain and faience factories to produce "equivalents" [1–8]. However, it is less known that the polychrome decoration of Chinese and Japanese porcelain is the result of the transfer of European enamelling techniques to Asia by missionaries, mainly Jesuits, at the end of the 16th in Japan [9] and of the 17th century in China [10–20], respectively. Not only were the recipes imported from Europe but also the ingredients and some craftsmen, as established by French and Chinese historical records [10–13,15,16,21].

One aspect of the preparation of enamels is the addition and adjustment of fluxes to enable them to be vitrified (these are mainly alkali ions (sodium and potassium), alkaline earth ions (calcium and barium), but also lead, boron as well as arsenic and phosphorus). If an abundant literature is interested in measuring the contents of sodium, potassium, calcium and lead in enamels (see for example the series of books published by Kingery [22,23]), because of the lack of analytical techniques for measuring them, very few work focus on lithium and boron even if the use of borax, a natural product containing these elements, is mentioned in many ancient French recipes [24,25].

In traditional techniques, the glaze "powder" applied on the object's surface before firing combines the "*corpo*" which constitutes the bulk of the silicate matrix (90 % and more by weight) with the "*anima*" which contains the colouring agents (transition metal ions or metal nanoparticles for periods prior to ~1850–1880) [26,27]. The "*corpo*" is a ceramic preparation based on pulverized natural raw materials (quartz, flint, feldspar/pegmatite, kaolin, chalk, etc.), while the "*anima*" is prepared with a mixture of silicates and colouring agents. The elements which generate the liquid phase during firing (Li, Na, Ca, Ba, B, Pb, As,

* Corresponding author.
E-mail addresses: jacques.burlot@hotmail.fr (J. Burlot), philippe.colomban@sorbonne-universite.fr (P. Colomban), ludovic.bellot-gurlet@sorbonne-universite.fr (L. Bellot-Gurlet), quentin.lemasson@culture.gouv.fr (Q. Lemasson), laurent.pichon@culture.gouv.fr (L. Pichon).

https://doi.org/10.1016/j.jeurceramsoc.2024.116746
Received 22 May 2024; Received in revised form 5 July 2024; Accepted 11 July 2024
Available online 16 July 2024

P) are present in both preparations. The elemental composition of the "final" enamel will differ from that of the starting powder because the elements that are volatile at firing temperatures, namely Li, B, Pb and As, are partially lost during the process. Furthermore, smaller cations, such as lithium, easily diffuse deep into the substrate. Given the intrinsic heterogeneity of the decoration obtained, a "global" composition does not specifically characterise the colouring agents (and especially those present in the form of pigment grains), which underlines the need to be able to grasp the volume on which the analytical technique collects information, in particular for the non-invasive examination [28–31].

If in some cases (when similar archaeological shards existing in large numbers) it is possible to use precise but destructive techniques such as XRF analysis on borax-based glass pellets [32], LA-ICP-MS [33] or LIBS [34], the analysis of rare objects requires the use of non-invasive techniques, which therefore only probe surfaces or quasi-surfaces. Moreover, because of the high costs of conditioning, transporting and insuring heritage objects, these analyses must be carried out on the conservation site with mobile instruments such as Raman microspectroscopy [28–31, 35,36] and pXRF [28–32], or with instruments installed in the conservation site (as in the case of the particle accelerator used in our study [37,38]). Among the techniques commonly used to characterise the elemental composition of ceramics (such as XRF, SEM-EDS, INAA, ICP-MS, etc.), few allow the determination of light elements such as Li and B. The techniques that do allow this are ICP-MS, LIBS, Prompt Gamma Neutron Activation Analysis (PGNAA) and Particle-Induced Gamma-ray Emission (PIGE). PGNAA does not allow local analyses, while ICP-MS, even in its laser ablation version (LA-ICP-MS), and LIBS are micro-destructive. Only PIGE allows non-invasive measurement of Li and B in ceramics, which is mandatory for the analysis of rare objects.

We present here the PIXE/PIGE analysis conducted at the New AGLAE facility on porcelain and plates representative of 18th century Chinese and French productions. This work is preliminary to the examination of series of imperial objects previously studied on site by pXRF and Raman scattering [14,29–31]. This makes it possible to measure B and Li (by PIGE) as well as the remaining elemental composition (by PIXE) at the same analysis point, which is useful for highlighting possible correlations in these very heterogeneous samples. Ancient recipes [17,24,25,39] and for rare samples, the non-invasive Raman analysis technique [40] previously suspected the presence of borate in the enamels. If the use of borax, a natural compound of complex composition ($Na_{2-x}Li_xB_4O_7.10\ H_2O$) generally collected in salt lakes and geothermal deposit (e.g. in Turkey and Tibetan plateau) [41–43], is fairly well documented in recipes [17,24,25,39], detecting its use in enamels by measuring B or Li is not achievable by most non-invasive methods. This is also the case for Na, which is difficult to quantify using the most commonly used mobile non-invasive elemental analysis technique with portable X-ray fluorescence (pXRF) instruments. This is because it requires devices with a measurement environment that limits the presence of air, which is achieved by using a vacuum pump or Helium flow. Another way to detect the presence of B is through structural characterisation of boron-containing phases using Raman microspectroscopy, which can detect the B-O bonds and different BO_3 and BO_6 species [44–48], but this is generally best achieved using a special laser excitation (in the blue) that is not available with mobile instruments. The results obtained by Raman analyses [40] showed a strong heterogeneity in the distribution of boron in the glazes, explained by its volatility and by the very small thickness of the overglazed enamels, of the order of (a few) tens of microns.

2. Materials and methods

2.1. Samples

The shards and the plates analysed are shown in Fig. 1. Information on their origins is summarized in Table 1 and more detailed information can be found in previous publications reporting their analysis by Raman

Fig. 1. Samples and artefacts analyzed by PIXE/PIXE analysis (see references [25,40,49,50] for details on the shards and artefacts).

microspectroscopy, optical microscopy, SEM-EDS and/or pXRF [40,49, 50]. The choice was made among porcelains already analysed by different techniques as part of a program to study European glazing/enamelling techniques and their transfer to Asia by missionaries, particularly the Jesuits, at the end of the 16th century in Arita (Japan) and at the end of the 17th century in Canton and Beijing (China) [9,14–20, 28–31]. In these objects, the use of borax in certain overglazes is documented or suspected [40,49,50], and in some spots, Raman analysis using a blue laser has detected vibrational modes compatible with an attribution coming from the BO_3 or BO_6 entity [44,48].

The stratigraphy of the ceramic decorations is complex, as is their distribution (owing to the fineness of the designs), which makes them difficult to characterise analytically (see Fig. 2 for a schematic cross-section). The thickness of the (under-)glaze or transparent enamel varies between 300 and 600 μm [25,36,40,50,51]; this layer being usually fired at the same time of the paste. The thickness of the overglazes or enamels, such as black or red lines used to structure the drawing, is much thinner, ranging from 30 to 100 μm [25,36,40,50,51]. In some cases, several layers of overglaze can be superimposed. For the measurements carried out and the objects considered in this study, it is assumed that the "probed" surface areas are homogeneous (representative of the same stratigraphy). However, this is certainly not always the case, because certain decorative techniques derived from miniaturist techniques use millimetre dots of variable colours, and one dot may contain several pigments or colouring agent [29–31]. These considerations concerning thicknesses and stratigraphy are decisive for the exploitation of analyses using irradiation or illumination from the surface. In fact, the excitation beam is progressively absorbed by the sample and therefore explores a given depth, and the radiation produced during the interaction is then more or less absorbed before emerging from the sample and reaching the detector [28].

The set of coloured areas analyzed is summarized in Table 1. The selected objects are a soft-paste porcelain with polychrome floral decoration produced at Sèvres Royal Factory in 1781, already analyzed by different methods [25,39,49], and six Chinese porcelains produced during the reign of the Kangxi (Imari-like dish, ca. 1700–1720), Yongzheng (*Famille* rose, ca. 1723–1735) and Qianlong (1735–1796) Emperors [40,50]. The samples were chosen to cover the 18th century and the different enamelling techniques (blue-and-white, polychrome decoration and gilding), and to include areas where the use of borax had previously been suspected.

2.2. PIXE and PIGE analysis

PIXE/PIGE analysis were conducted at the New AGLAE ion beam analysis facility [52]. An external microbeam of 3 MeV protons allows the simultaneous measurement of X-rays (PIXE) and gamma-rays (PIGE) emissions. PIXE analyses were performed with four X-Ray detectors, one with a flow of helium in front dedicated to the measurement of light

Table 1
Analysed samples. Areas in which boron was suspected are underlined and in bold. See Supplementary Material and Fig. 2 for details.

Sample labels	Origin (date)	Analysed area	Number of measure	Measure label	Previous analyses	Refs
MAG	Sèvres Factory (1781) Soft-paste porcelain	white (colourless glaze)	1	10	Raman, SEM-EDS, XRF	[25,39,49]
		dark blue	3	9,11,12		
FR	Yongzhen reign (1723–1735) *Famille rose* hard-paste porcelain	blue	2	18,19	Raman, SEM-EDS	[50]
		white	1	20		
		gilding	2	21,22		
		pink (rose)	2	23,24		
		black line	1	25		
QL	Qianlong reign (1735–1796) imperial bowl	**dark blue**	3	32,33,39	Raman, SEM-EDS	[50]
		white overglaze	3	34,41,48		
		black line	2	36,38		
		pale yellow green	2	42,43		
		yellow	2	44,40		
		pink	3	40,47,49		
		glaze (colourless)	1	41		
		red (background)	2	35,37		
BPL	Qianlong reign (ca. 1780) blue-and-white porcelain with weeping willow decoration	dark blue	3	13,14,15	Raman, SEM-EDS	[40]
IMARI	Kangxi reign Porcelain (1770–1720) (Imari copy)	dark blue	2	16,17	Raman, SEM-EDS	[40]
		white (colourless glaze)	1	69		
		gilding	2	67,68		
LAC	Qianlong reign (ca 1740–1750) *Famille rose* porcelain with lake landscape decoration	red	1	30	Raman, SEM-EDS	[40]
		gilding	2	26,28		
		white (colourless glaze)	2	27,31		
		black line	1	29		
ROSE	Qianlong (ca 1770) *Famille rose* porcelain with rose flower decoration	**blue** and black line (map)	1	64	Raman, SEM-EDS	[40]
		blue, black line and white (colourless glaze) (map)	1	65		
		black line and pink (rose) (map)	1	66		

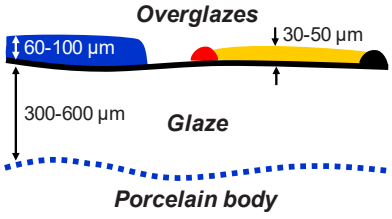

Fig. 2. Schematic sectional view of porcelain covered with glaze and overglaze. Typical thicknesses are shown.

elements and three carrying 50 µm Al filters for measuring heavy elements. The PIGE spectra were recorded using an unfiltered High Purity Germanium (HPGe) detector.

We use a 50 µm diameter beam and in order to homogenise the measurements over a small area considered to be homogeneous, the beam is continuously scanned over 500 µm during each acquisition. Sufficient counting statistics (especially for PIGE spectra) are obtained with analysis times between 3 and 5 minutes per measurement point. Fig. 3a and b shows the details of the external beam setup and its multi-detector system, and Fig. 3d-l give some examples of the rectangular analysis zone made visible by the luminescence of the sample under the proton beam.

The software suite developed by the AGLAE team not only drives the acquisitions but also quantifies the PIXE measurements using GUPIX [53,54]. Measurements and their accuracy are monitored using nine standards (NIST 93a, MA-N, Brill-A, Brill-B, Brill-C and BGIRA3) analyzed under the same conditions [55–57]. The representative PIXE spectra of these standards are shown in Fig. 5 and according to previous measurement campaigns the composition determined is close to the recommended values (error from 5 % to 10 % according to the element (Fig. 4).

PIGE measurements are quantified by calibrating the gamma emission response of boron and lithium with the NIST 93a and MA-N standards, respectively. For lithium, it is the emission at 478 keV (from nuclear reaction: $^{7}Li(p,p'\gamma)^{7}Li$) and those at 429 keV (from reaction: $^{7}Li(p,n_1\gamma)^{7}Be$). The latter cannot be separated from the boron emission at 429 keV (from reaction: $^{10}B(p,a\gamma)^{7}Be$), as the instrumental resolution does not allow the contributions to be separated. In this energy window, we also have the contribution of gamma-ray emission from Na at 440 keV (from nuclear reaction: $^{23}Na(p,p'\gamma)^{23}Na$), which partly overlaps the peak at 429 keV. As discussed later, to assess the presence of boron despite spectral interference on the peak at 429 keV when boron and lithium are present, the intensity ratios of the peaks at 478 keV (Li) and 429 (Li and B) are calculated. To quantify Na, Li and the contribution (Li+B), three evaluations are performed. Two of these are based on a Lorentzian adjustment of the peaks to obtain their areas and intensities, which are used separately. The third evaluation is carried out by recording only the intensity at the maximum of each of the peaks (which will be called the "intensity at maximum").

Given the multi-layered structure of the samples analysed, as well as their variable composition, which is often rich in heavy elements such as lead, the question of the depths at which the various elements are probed is a major concern. The depth probed by the PIXE analysis is estimated using the GUPIX software [54], assuming 90 % absorption of the incident proton beam and of the X-ray fluorescence emission. Table 2 gives the penetration values according to the elements considered in this study and the two typical silicate matrices encountered, with and without lead. We note that, as expected, the characteristic depths probed are approximately twice as weak as in analysis of X-ray Fluorescence excited by X-rays (XRF) [28,58] because the proton beam path is much more circumscribed than that of the X-rays conventionally used in XRF (this is due to the different interaction mechanisms of protons and X-rays in matter). More generally, for complex samples, PIXE measurements can be quantified more reliably than portable X-ray fluorescence measurements because the proton pathway in the sample is well modelled and more limited than for X-rays.

PIGE analysis, on the other hand, is much less affected by issues of self-absorption of gamma emissions and variations in matrix composition, and probes a depth of around 70 µm, which corresponds to the path of the protons. This lower absorption of gamma rays compared to X-rays means that we can obtain compositions that are not solely representative

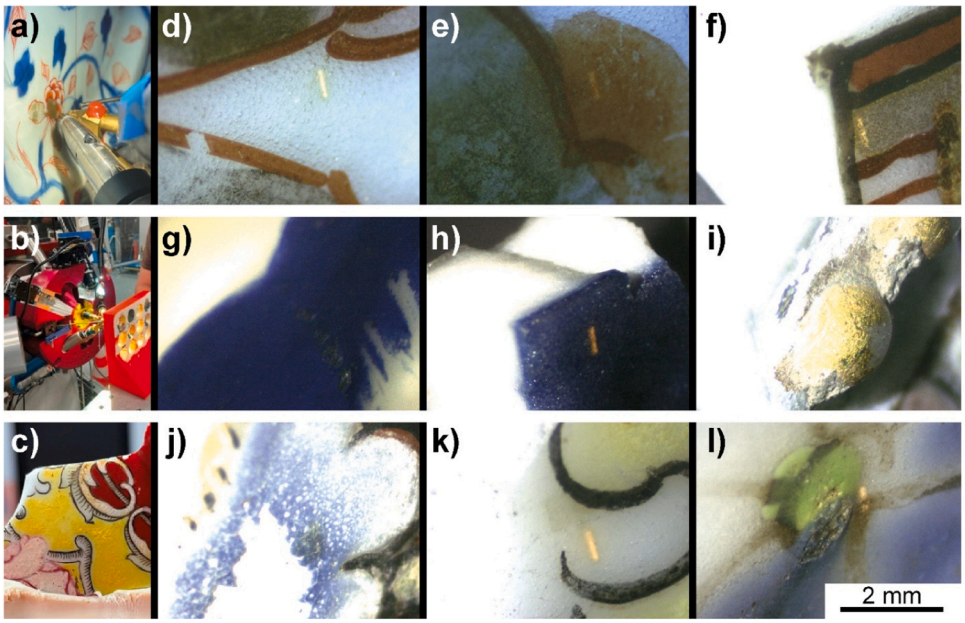

Fig. 3. View of the extracted beam analysis facility (beam exit, X-ray and gamma detectors, cameras) during the positioning of the IMARI plate (a), of the standards (b), and detail of the positioning of a shard pasted on a support (c). A camera allows observing the rectangular area irradiated highlighted by the yellow luminescence induced by the scanning of the beam (~50×500 μm^2). An example is shown for each shard or object analysed (d-l): d-e) IMARI; f) LAC; g) MAG; h) BPL; i) FR; j-k) QL; l) ROSE. See more details on samples in reference [40,50].

of the extreme surface (see Table 2 for depths probed by X-rays). The volume probed and the compositions determined by PIGE are therefore less influenced by the mechanisms or alterations affecting the surfaces.

PIXE and PIGE measurements/quantifications are therefore less affected by the multi-layer structure of the objects studied. Considering the typical stratigraphy (Fig. 2) and the estimated depth of analysis (Table 2), the signals of the elements studied will be well representative of the coloured surface layer (glaze or overglaze), without notable contribution from the underlying layer. In addition, the high gloss of the studied enamelled surface guarantees an absence of significant corrosion, which means that there is no significant loss of alkaline ions by leaching to take into account. On the other hand, it is likely that a surface loss of volatile elements (lithium, boron, or even sodium) at the firing temperature may occur.

3. Results

3.1. Comparison of "standard" flux content and identification of the different enamelling technology

We start by looking at the "standard" flux elements, i.e. without considering B and Li, which provide an initial definition of the types of enamelling technologies. Fig. 5 presents representative PIXE spectra from studied artefacts and some of the colour analysed. The presence of lead is obvious for overglazes/enamels that were fired at relatively low temperature, i.e. in the 600–1000°C range. On the contrary, no lead is detected for blue area of Imari-like porcelain, the blue *décor* having been directly painted on the porcelain body before the application of the glaze. Peaks characteristic of calcium are also detected in most of the studied areas, with the exception of samples/zones MAG white and QL yellow, due to their high content of lead.

The strong signal of manganese (Kα) in the blue of the Chinese copy of the Imari decoration (Japan) (Fig. 5c) is characteristic of the use of cobalt ore of Asian origin [29–31,50,59]. The strong iron content in the red enamel of LAC sample (Fig. 5e) is characteristic of the use of hematite [40]. These results are in agreement with previous analyses. We note that the detection of arsenic opacification is clear although, as in XRF, only the weak As Kβ peak (close to 12 keV) can be observed due to the confusion of the Pb Lα and As Kα peaks (Fig. 5g). The contribution of arsenic is also clearly quantified, as shown in Fig. 6e.

The pXRF measurements provide reliable assessments of the presence of these elements, but as mentioned above, for the samples studied, the PIXE measurements have the advantage of providing a more representative measurement of the upper layers only (i.e. the painted enamel decorations/overglazes). The results obtained can therefore be considered to be more meaningful in terms of raw materials and glaze technologies.

To compare the flux contents of the different enamels analyzed, we use the ternary diagrams featuring the oxides that favour the formation of liquid phase (and therefore the vitreous phase) and that are well documented in the literature (phase diagram for ceramists [60]), namely PbO, Na_2O and CaO, but also P_2O_5 and arsenic oxide, which can also play the role of flux (Fig. 6). The variability of the element content plotted in Fig. 6 (PbO, Na_2O, K_2O, CaO, P_2O_5, As) concerning the same coloured zone is attributed, firstly, to the heterogeneity of the coloured zone itself, secondly, to variations in the concentration close to the surface (gradient due to evaporation loss during the firing) and, thirdly, to variations in the thickness of the enamel layer (overglaze) which induces a variable contribution from the substrate. Consequently, the data appear aligned on a straight line coming from the PbO pole with an almost constant Na_2O/K_2O (Fig. 6a) and CaO/K_2O ratio (Fig. 6b). However, we observe the same conclusions as those of previous SEM-EDS analyses [25,40,50]: the blue decorations of BPL and Imari objects are without lead, the gold decorations of FR are almost free of PbO and the yellow areas of QL are very rich in PbO due to the use of pyrochlore yellow pigment.

The variability observed in the CaO content (Fig. 6) makes it possible to identify the three different enamelling technologies: i) the underglaze decoration (BPL and IMARI), ii) the decoration with a low addition of lead (LAC and the red background, the black lines of QL and pink of FR), and iii) enamels rich in lead (yellow of QL, blue of QL and MAG). The presence of P_2O_5 characterizes the blue BPL decoration (not reported in XRF studies, where this element is more difficult to detect than in PIXE), which is free of arsenic, a typical characteristic of the use of "Asian" cobalt [59,61–63], while the evidence of a low level of arsenic for the QL and FR enamels confirms the use of ingredients imported from Europe

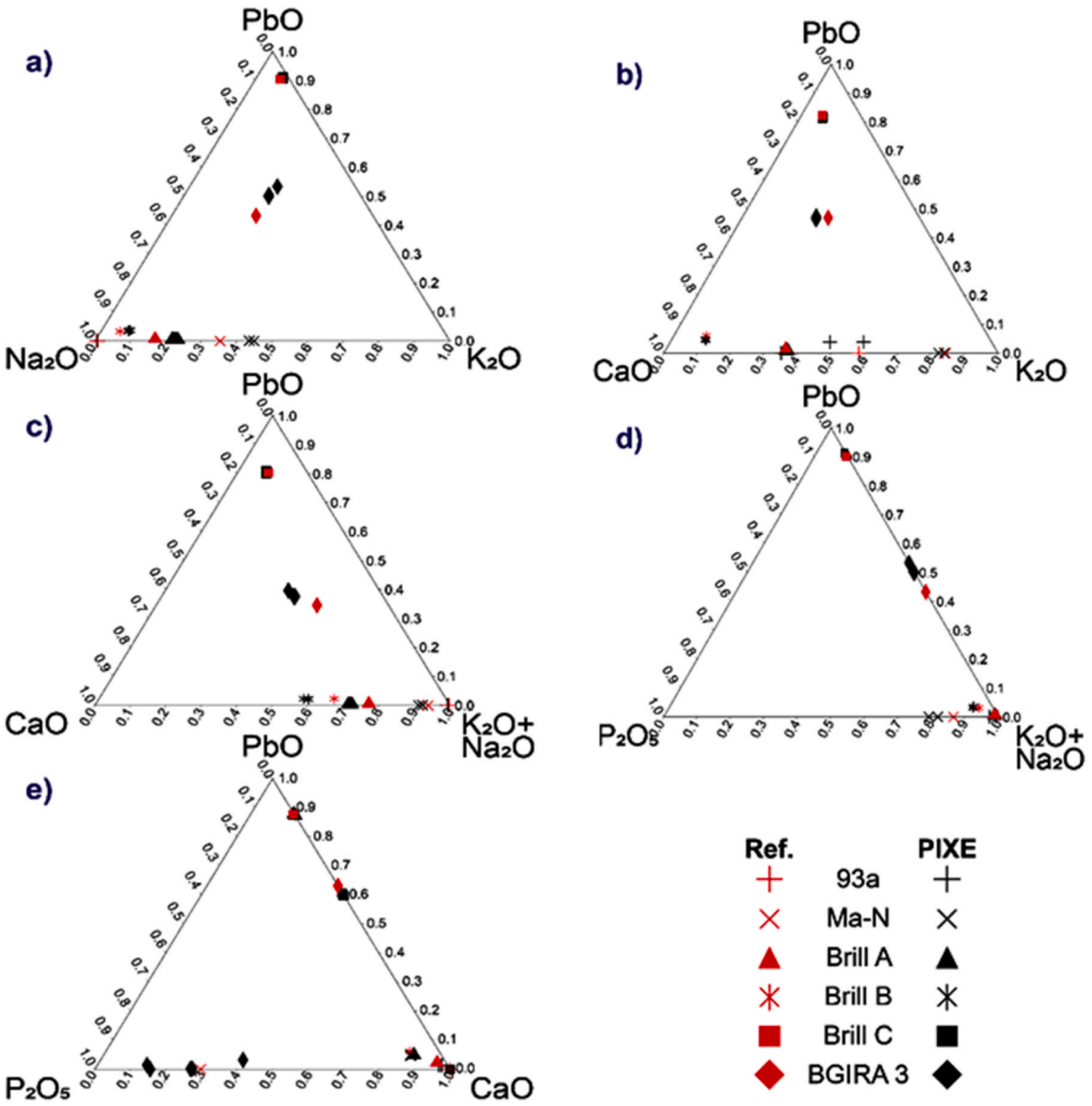

Fig. 4. Comparison of the clustering of flux oxides contents obtained from PIXE analyses (black symbols) and certified compositions (red symbols) of the reference standards (compositions are given in Appendix, Table A1).

Table 2
Depths analyzed by PIXE estimated by GUPIX software for some elements and for two types of matrix (Brill B and Brill C standards), taking into account the absorption of the excitation ion beam and the emitted X-rays.

Element XRF transition	Li and B K	Na	Si	K	Ca	Transition metals	Pb L	Sn K	Sb K	Remark
Depth (μm)	<1	1	4	5	3	30–45	45	44	45	(Pb-free) glaze (Brill B)
	<1	1	4	5	6	13–30	40	46	46	Pb-overglaze (Brill C)

[28–31,62–66].

3.2. Search of lithium and bore content

Fig. 7 shows representative PIGE spectra showing the respective peaks of sodium at 440 keV, lithium at 478 keV, and the peak common to boron and lithium at 429 keV. In the energy range containing these three peaks, we can thus qualitatively separate the samples (artefacts and standards) into four groups on the basis of their spectra:

i) Sodium only: glazes of MAG sample (see Appendix, Table A2, #09–12).
ii) Sodium and lithium, but no boron as its main peak at 429 keV is not detected: all enamels and the underglaze of IMARI (#16–17, #67–69), BPL blue (#13), FR gilding (#21–22), LAC gilding, red and underglaze (#26, #30 and #27, respectively), QL white (#34, #41 and #48). We also include standard MA-N in this group since we know its composition, including ~6 wt% Na_2O and ~0.5 wt% Li but no boron (see Table A1 for its whole composition); the peak then observed at 429 keV (Fig. 7h) thus corresponds only to the presence of lithium.

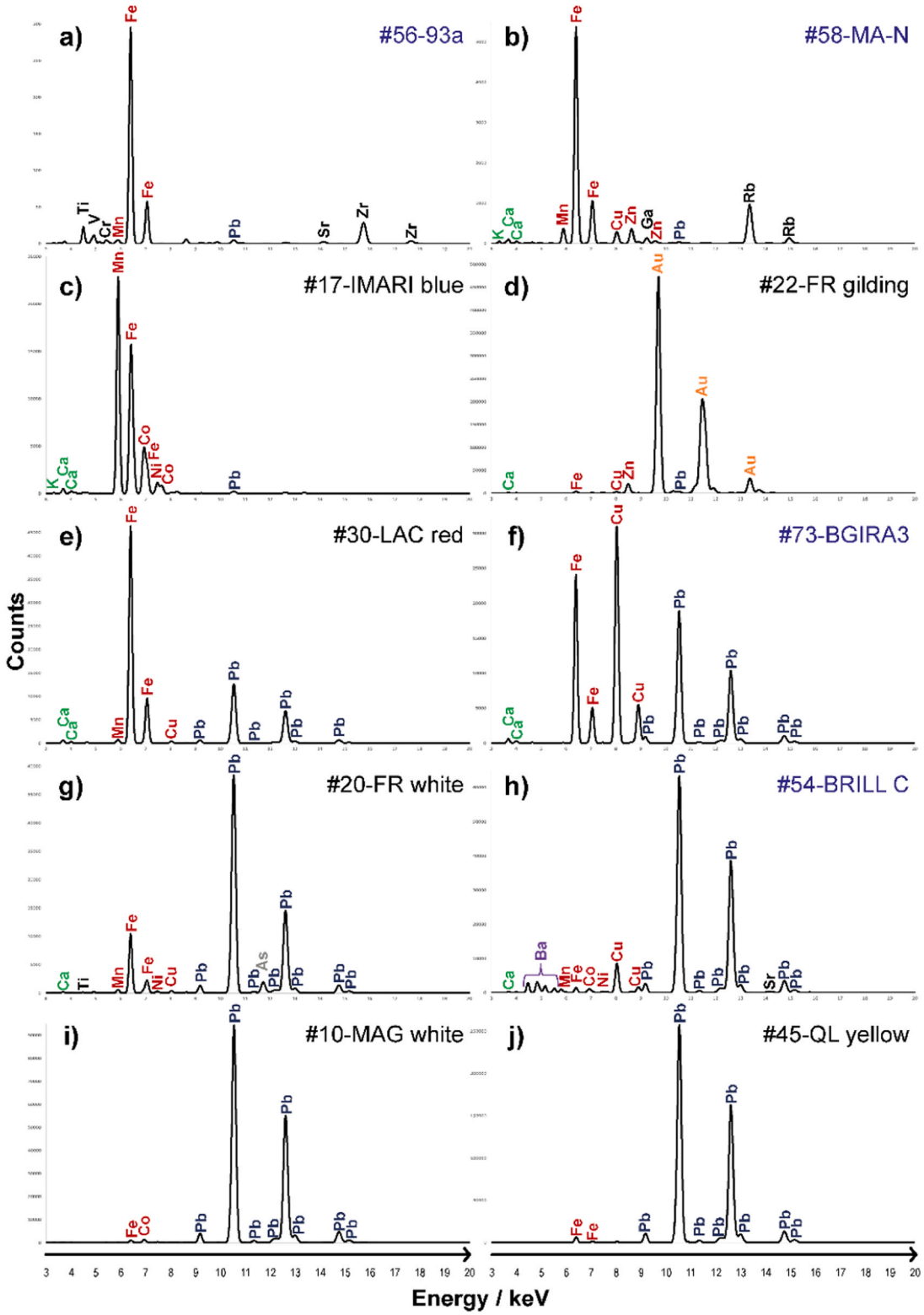

Fig. 5. Representative PIXE spectra of reference samples (NIST 93a(a), MA-N (b), BGIRA3 (f), BRILL-C (h)) and artefacts (IMARI (c), FR (d,g), LAC (e), MAG (i) and QL (j)). Colours of studied area are given (see Table 1).

iii) Sodium, lithium and possibly boron since the mixed Li-B peak at 429 keV has a relative width or intensity compared to the "pure" peak of lithium at 478 keV: FR blue, white, pink and black (#18–19, #20, #23–24 and #25, respectively), BPL blue (#14–15), LAC gilding, black and underglaze (#28, #29 and #31, respectively), and QL blue, yellow, green, red, pink, black and underglaze (#32–33,39, #44–45, #42–43, #35,37, #40,47,49, #36,38 and #46, respectively).

iv) Sodium and boron, but no lithium as its main peak at 478 keV is not detected: this group includes only the standard NIST 93a which contains 12.56 wt% B_2O_3 and 4 wt% Na_2O (see Table A1 for its whole composition).

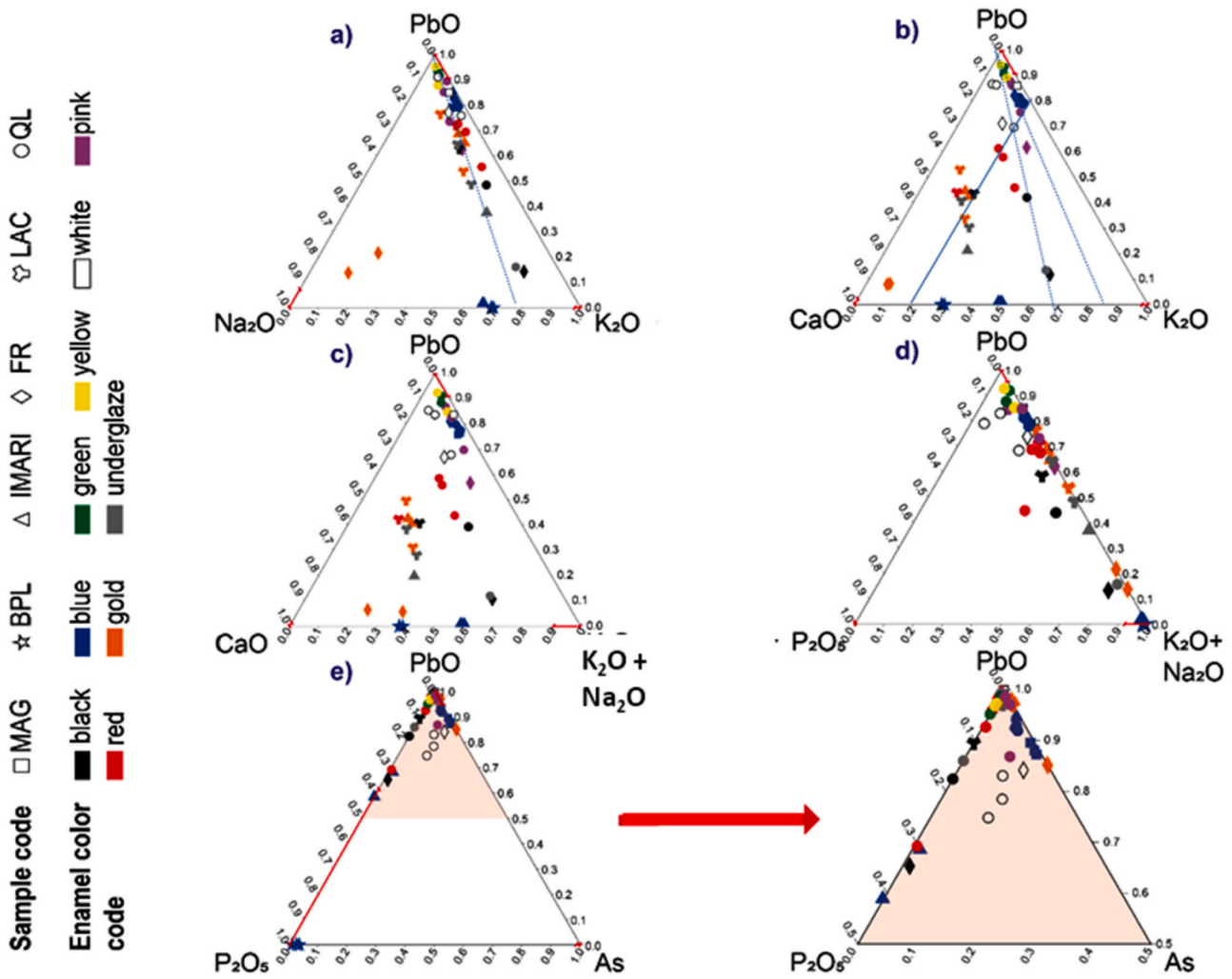

Fig. 6. Comparison of the clustering of flux oxides contents obtained from PIXE analyses of coloured enamels. The label colour corresponds to the colour of area analyzed for each artefact/shard. Sea Table 1 for explanation of labels. For e) a zoom of the upper part of the diagram is given on the right.

From this visual observation of the PIGE spectra (Fig. 7), we can think that only enamels in group iii) may contain boron, because of the peak at 429 keV. However, we cannot be certain of the presence of this element, since no other boron PIGE peaks were detected, notably at 718 and 2125 keV [for $^{10}B(p,p'\gamma)^{10}B$ and $^{11}B(p,p'\gamma)^{11}B$ nuclear reactions, respectively, bearing in mind, however, that these reactions have significantly lower cross-sections], and all the samples in this group also contain lithium; thus the 429 keV peak could only represent the secondary peak of the latter.

To determine whether boron was present in the glazes of group iii), we decomposed the spectra and calculated the ratio of the intensity of the 478 keV peak to that of the 429 keV one. We did the same with the MA-N standard to obtain a reference ratio of the relative intensity of these two lithium peaks, since this sample contains lithium but no boron. The calculated ratios of the 478 keV/429 keV peaks are shown in Fig. 8. In this representation, the lower the ratio, the more the intensity of the peak measured at 429 keV is influenced by the presence of boron.

In Fig. 8, group A, we can thus see that three enamels have ratios between 4.5 and 5.5, similar to those calculated for the MA-N standard without boron. These are FR blue (#18), QL blue (#33) and yellow (#45), for which we therefore consider that only lithium is present. Doubts as to the presence of boron arise for the samples in group B of Fig. 8, as their ratios are relatively high, between 3.1 and 4.3. These are FR's second blue enamel (#19), LAC's three enamels (#28–29,31) and QL's two remaining blue enamels (#32,39), as well as its second yellow enamel (#44) and one of its two green ones (#42). For the samples in group C in Fig. 8, whose ratios are below 3, we consider that they contain lithium and boron. These samples include two BPL blue enamels (#14–15), FR's white, pink and black enamels (#20,23–25), as well as one of QL's two green enamels (#43) and all its pink, red and black ones (#35–38,40,47,49) plus its underglaze (#46).

In a second step, we compare the sodium, lithium and possibly boron contents calculated from the area and the height resulting from the fitting of the three peaks at 429, 440 and 478 keV using ternary diagrams (Fig. 9a-b). A third evaluation is shown in Fig. 9c, based on the "intensity at the maximum" of each peaks.

Examination of the ternary diagrams built with the two first procedure (Fig. 9a-b) shows three groups of data, those aligned on the Na-Li line (Imari, QL white, one BPL blue and MAG), and two separate groups shifted on the Li/B pole side. The clustering of these groups look clearer on the diagram constructed using the height obtained by the peak fitting (Fig. 9b). We will therefore first discuss this diagram (Fig. 9b).

The samples which contain the most boron are expected to be those for which the height of the mixed peak is maximum, which is normal but cannot be considered as infallible proof of the presence of boron when the offset is small. These data concern many colour of the QL sample and to a lesser extent those in the FR sample. Certain colours, such as pinks (colours obtained by the dispersion of gold nanoparticles), are shifted on the Li/B pole side, which can therefore be considered as proof of the presence of boron.

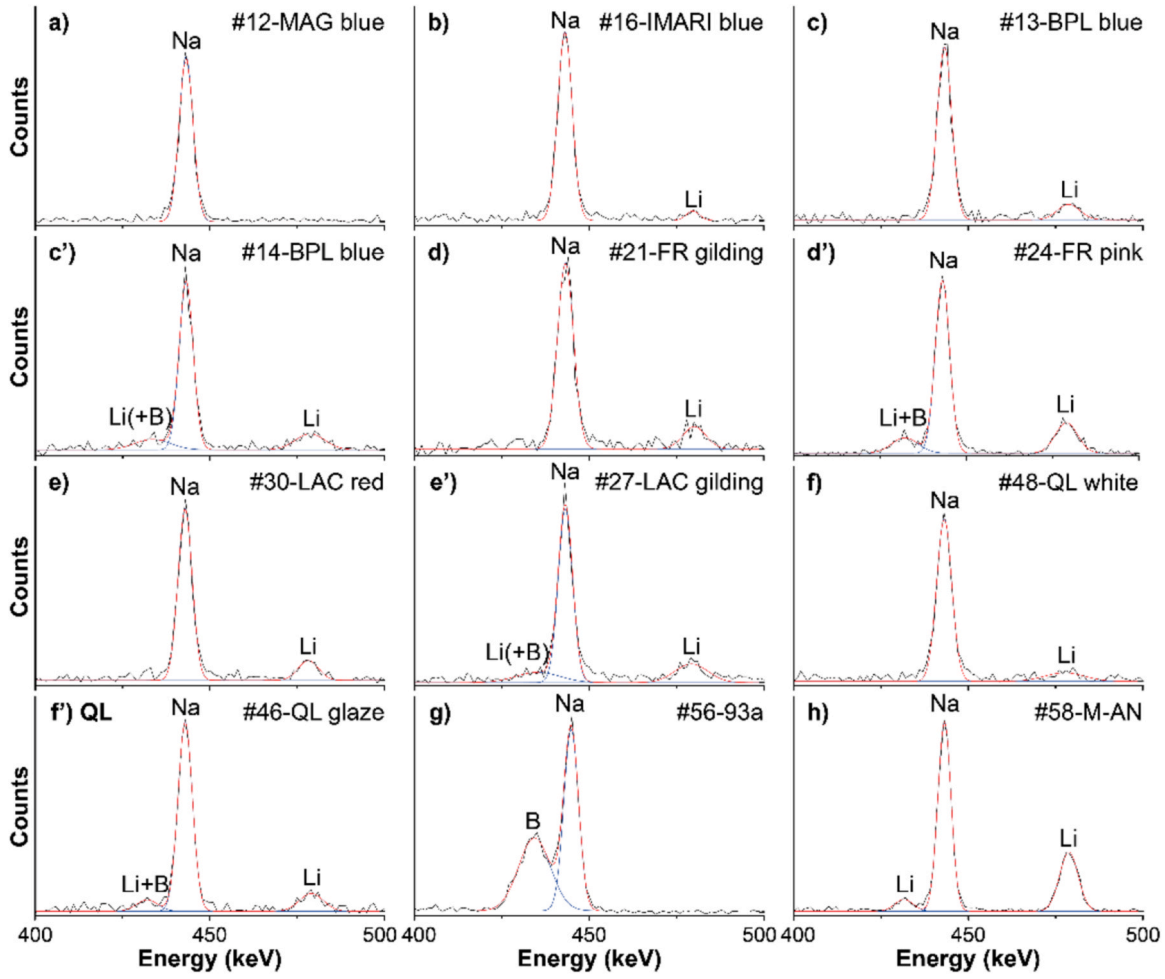

Fig. 7. Representative PIGE spectra showing the main Na, Li and B peaks: a-f') samples; g-h) reference standards; see Table S1 for composition of references.

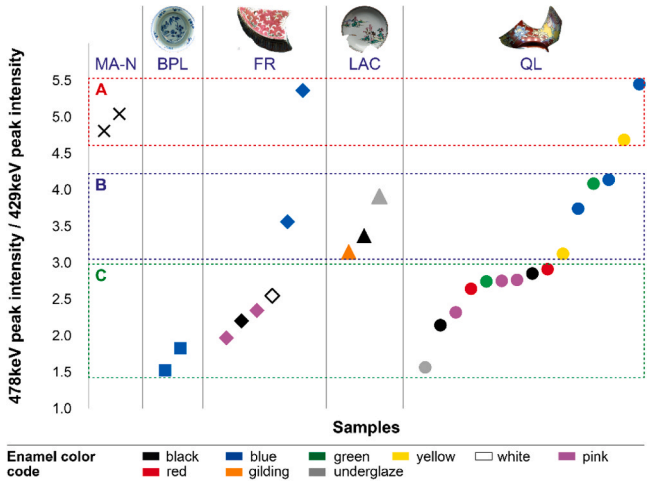

Fig. 8. Ratio of the intensity of the 478 keV Li peak to that of the 429 keV (Li+B) peak calculated after the fitting of PIGE spectra. It concerns only enamels for which the PIGE spectrum features these two peaks, plus the reference standard MA-N (containing Li and no B) for comparison.

The ternary diagram constructed from the intensities at peak maximums (Fig. 9c) shows a larger offset towards the Li/B pole side. The same type of shift can also be noticed for the data obtained on the blue zone of the MAG shard, where the Raman spectrum in certain places of these blue zones shows a Raman signature characteristic of a boron glass [40]. More generally, the zones analysed for the other shards were also shifted in Fig. 9 diagrams, only the IMARI sample appears to be definitely free of boron.

4. Conclusions

The search for an unambiguous and non-invasive evidence of the presence of boron in enamels appears to be a difficult issue by PIGE, especially at low levels associated with the presence of lithium (which produces an emission that interferes with the main emission of boron), as is the case here. On the contrary, the demonstration of the presence of lithium is without discussion, since one of its gamma emissions is measured without spectral interference. The uncertainties about the presence of lithium are not only analytical but arise from the characteristics of the glazes and the temperature behaviour of the lithium ion during firing. Due to its small size, which allows it to diffuse very rapidly in the environment, in the liquid, solid and gaseous phases, its residual presence in the glass can be affected. The final content in the enamel is therefore necessarily lower than that of the "enamel" powder deposited before firing. With the exception of borax, virtually no other raw material can provide significant amounts of lithium. Also the detection of this element must be considered as an indication of the addition of boron in a glaze.

In the present case, the non-invasive PIGE analysis revealed the presence of sodium and lithium in all the Chinese enamels, as well as boron, systematically in the two colours pink and black. Boron was detected in other colours, except gilding, but not for all samples

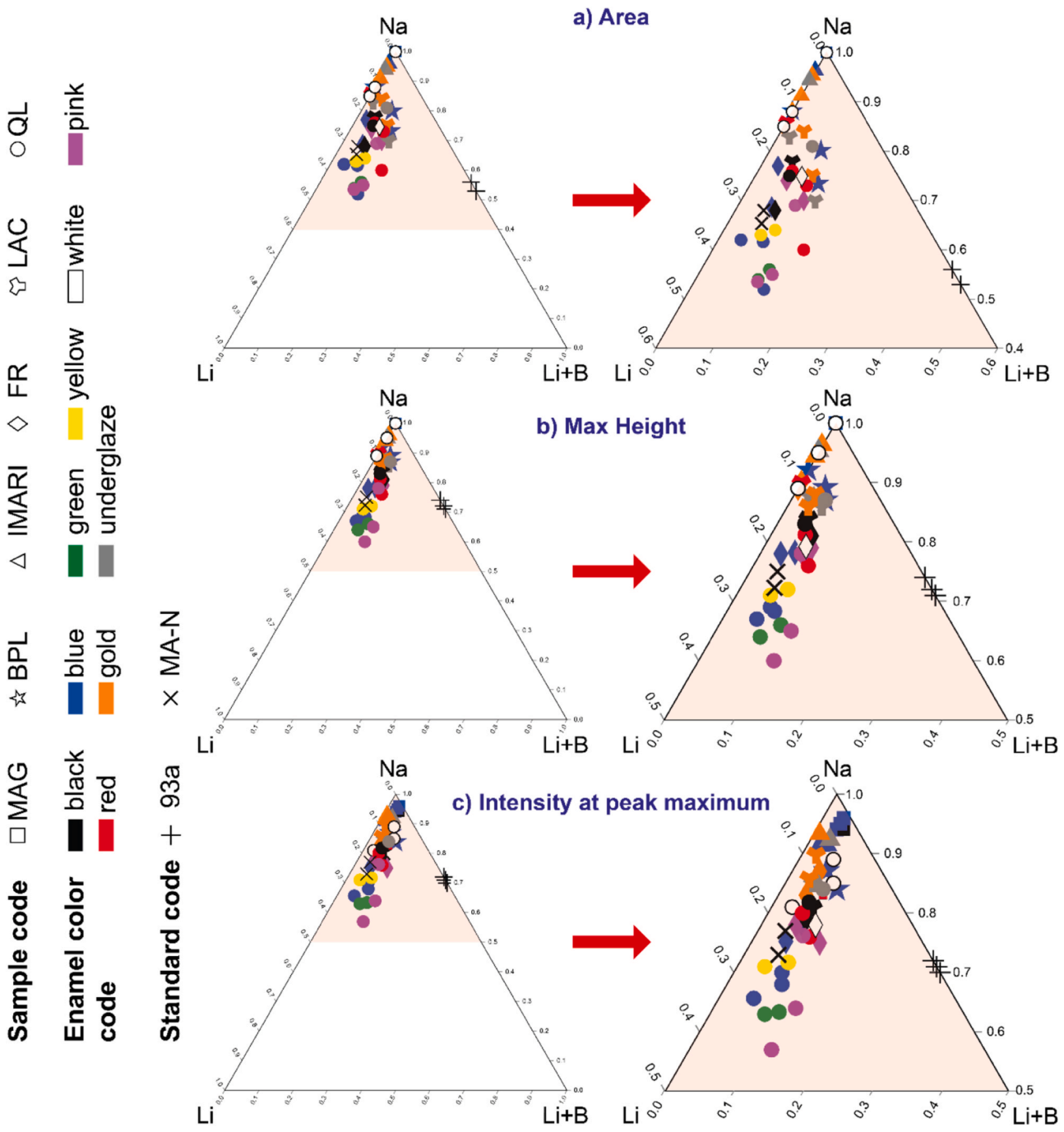

Fig. 9. Comparison of the clustering of (Na, Li, B) flux elements content obtained from the PIGE spectra of coloured enamels using 3 different procedures: fitted peak area (a), fitted height (b) and intensities at peak maximums (c) (See Table 1 for explanation of labels). The diagrams on the right are enlargements of those on the left.

(Table A2). These results confirm the findings of the Raman micro-spectroscopy analysis, which detected borate phases in some of these enamels. For the French sample (MAG), although borate phases were detected episodically by Raman spectroscopy in some blue glazes, neither boron nor lithium was detected in the present study. This could be explained by the heterogeneous distribution of boron in the enamels and the fact that not exactly the same points were analysed by PIGE and Raman spectroscopy. This question of homogeneity of composition is true for this sample, but also for painted enamels in general, whose compositions are intrinsically heterogeneous. Sample BPL for example, features both lithium and boron in two of the blue spots analysed, while only lithium was detected in a third one.

These issues of the representativeness of the analyses suggests that a greater number of analyses over large areas (approaching the scale of the decorations) would optimise the chances of detecting traces of borax and provide a more representative set of compositional data. Non-invasive spot analysis using PIGE can be used to produce such elemental maps, the only limitation being the total analysis time required by the multiplication of analysis points, while maintaining counting times that allow B and Li to be detected.

LA-ICP-MS is currently the other analytical approach that allows the spot measurement of elements such as B and Li. It enables these elements to be detected very effectively, and also allows a certain depth to be probed in the sample as the ablation proceeds, enabling any surface-related heterogeneities to be assessed. However, the micro-craters created by ablation are unacceptable for rare ceramic objects such as

produced for the Chinese Emperor. This analytical approach would therefore only be possible on shards (not complete pieces), which could also be analysed on their section, without affecting their surfaces.

With regard to the other elements quantified in this work, compared to X-ray fluorescence analysis, PIXE analysis of glazes provides elemental compositions that are more representative of thin glass layers. As we have discussed, proton-matter interactions probe smaller volumes than X-rays and are better evaluated by the quantification software used (i.e. GUPIX). Although X-ray fluorescence analysis has the advantage that it can be carried out by portable instruments (i.e. in the field), its results can be more easily affected by the ceramic substrates of the enamel layers. For SEM-EDS analysis, they are limited in their ability to analyse large samples due to the limited size of their analysis chambers. Another advantage of the PIXE analyses carried out in this work, compared to previous data obtained using portable X-ray fluorescence, is the better detection of light elements such as phosphorus by PIXE (due to higher cross-sections of reaction with protons). This revealed the presence of phosphorus in some of the analysed enamels, adding to our knowledge of their constituents.

This work confirms the difficulty of non-destructive measurement of a group of widely used boron-based fluxes, which are nevertheless, mentioned in many ancient recipes that emphasize the use of borax. For the objects to be studied, the main constraint is the requirement for non-invasive analyses that can be carried out on small surfaces/volumes. As we have shown, PIGE analyses have interesting potential for this. However, the low amounts present and the gamma spectral interference between Li and B make it difficult to detect B in the presence of Li. However, as these elements are very likely to occur together in boron-rich raw materials, the presence of traces of lithium may be indirectly due to the addition of a boron-containing flux. The possibility of increasing the number of analyses of ancient objects should make it possible to better document the use of boron fluxes by the objects themselves. The specific behaviour of these light elements during the firing process would also require the use of elemental mapping to provide a statistically representative view of the presence/distribution of these light fluxing elements.

CRediT authorship contribution statement

Jacques Burlot: Writing – review & editing, Writing – original draft, Visualization, Validation, Formal analysis. **Laurent Pichon:** Writing – review & editing, Investigation, Formal analysis. **Quentin Lemasson:** Writing – review & editing, Investigation, Formal analysis, Data curation. **Ludovic Bellot-Gurlet:** Writing – review & editing, Validation, Investigation. **Philippe Colomban:** Writing – original draft, Visualization, Validation, Supervision, Resources, Project administration, Methodology, Investigation, Funding acquisition, Formal analysis, Conceptualization.

Declaration of Competing Interest

The authors declare that they have no known competing financial interests or personal relationships that could have appeared to influence the work reported in this paper.

Acknowledgements

We are grateful for the access to measurements offered by the New AGLAE facility (EQUIPEX ANR-10-EQPX-22, French Ministry of Research). This work was partially funded by the French Agence Nationale de la Recherche ANR EnamelFC project 19-CE27-0019-02.

Appendix A. Supporting information

Supplementary data associated with this article can be found in the online version at doi:10.1016/j.jeurceramsoc.2024.116746.

References

[1] M. Pirazzoli-T'Serstevens, La céramique chinoise en Italie, XIIIe-début XVIe siècle, Taoci 4 (2005) 75–86.
[2] E. Levy, Le Goût Chinois en Europe au XVIIIe Siècle: Catalogue du Musée des Arts Décoratifs, June–October 1910, Librairie Centrale des Beaux-Arts, Paris, 1910. ⟨https://gallica.bnf.fr/ark:/12148/bpt6k441547m/f1.texteImage⟩ (Available online).
[3] P. Verlet, Le commerce des objets d'arts et les marchands merciers à Paris au XVIIIe siècle, Ann 13 (1) (1958) 10–29, https://doi.org/10.3406/ahess.1958.2705.
[4] O. Impey, Collecting Oriental Porcelain in Britain in the Seventeenth and Eighteenth Centuries. The Burghley Porcelains, an Exhibition from the Burghley House Collection and Based on the 1688 Inventory and 1690 Devonshire Schedule, Japan Society, New York, Tokyo, 1990, pp. 36–43.
[5] J. van Campen, T.M. Eliëns, Chinese and Japanese Porcelain for the Dutch Golden Age, Waanders Uitgevers, Zwolle, 2014.
[6] S. Castellucio, Le prince et le marchand. Le commerce de luxe chez les marchands-merciers parisiens pendant le règne de Louis XIV, Kronos 73, Editions S.P.M., Paris, 2014.
[7] J. Finlay, Henri Bertin and the Representation of China in Eighteenth-Century France, Routledge Research in Art History, New York, 2020.
[8] A. Meyer, L.V. Esterhuizen, A southern African perspective of the early Indian Ocean trade, Chapter 4, in: S. Tripati (Ed.), Maritime Contacts of the Past. Deciphering Connections Amongst Communities, Delta Book Word, New Delhi, India, 2015, pp. 54–94.
[9] R. Montanari, N. Murakami, P. Colomban, M.F. Alberghina, C. Pelosi, S. Schiavone, European ceramic technology in the Far East: enamels and pigments in Japanese art from the 16th to the 20th century and their reverse influence on China, Herit. Sci. 8 (2020) 48, https://doi.org/10.1186/s40494-020-00391-2.
[10] C.-F. Shih, Evidence of East-West exchange in the eighteenth century: the establishment of painted enamel art at the Qing Court in the reign of emperor Kangxi, Natl. Palace Mus. Res. Q. 24 (2007) 45–94.
[11] C.-F. Shih, Hua Falang: The Chinese Concept of Painted Enamels, in: The RA Collection of Chinese Ceramics: a Collector's Vision, V, Jorge Welsh Research & Publishing, London, 2021, pp. 28–59.
[12] C.-F. Shih, L'Avènement d'une nouvelle palette de couleurs à Jingdezhen au XVIIIe siècle, in: P. d'Abrigeon (Ed.), Le Secret des couleurs. Céramiques de Chine et d'Europe du XVIIIe siècle à nos jours, 5 Continents Editions, Fondation Baurn, Milan, 2022, pp. 21–59.
[13] X. Xu, Europe-China-Europe: the transmission of the craft of painted enamel in the seventeenth and eighteenth centuries, in: M. Berg, F. Gottmann, H. Hodacs, C. Nierstrasz (Eds.), Goods from the East, 1600–1800 Trading Eurasia, Palgrave Macmillan, London, 2015, pp. 92–106.
[14] P. Colomban, Y. Zhang, B. Zhao, Non-invasive Raman analyses of Chinese huafalang and related porcelain wares. Searching for evidence for innovative pigment technologies, Ceram. Int. 43 (15) (2017) 12079, https://doi.org/10.1016/j.ceramint.2017.06.063.
[15] E.B. Curtis, Glass Exchange between Europe and China, 1550-1800. Diplomatic, Mercantile and Technological Interactions, Aldershot, Ashgate, 2009.
[16] E.B. Curtis, Aspects d'un processus protéiforme. La circulation des émaux entre le Vatican et la cour de Kangxi (1700-1722), Extr. ême-Orient - Extr. ême-Occident 43 (2019) 29–39, https://doi.org/10.4000/extremeorient.1596.
[17] H. Ma, J. Henderson, J. Cui, K. Chen, Glassmaking of the Qing dynasty: a review, new data, and new insights, Adv. Archaeomater. 1 (1) (2020) 27–35, https://doi.org/10.1016/j.aia.2020.11.001.
[18] Y. Xu, Painted Enamel on Ceramics - The Encounter of Dutch and Chinese Pottery. ⟨https://www.aronson.com/painted-enamel-on-ceramic-the-encounter-of-dutch-and-chinese-pottery/⟩, 2022, (Accessed 23 November 2022).
[19] J. Bellemare, A new palette: reassessing the development of enamel colors in early-eighteenth-century China, J. Glass Stud. 64 (2022) 147–167. ⟨https://www.jstor.org/stable/48703407⟩.
[20] P. Colomban, Tracer l'utilisation de recettes et/ou d'ingrédients européens dans les objets émaillés: stratégie et premiers résultats, Artefact 18 (2023) 161–193, https://doi.org/10.4000/artefact.13945.
[21] I. Landry-Deron, La contribution des missionnaires aux arts du feu à la cour de Pékin (XVIIe-XVIIIe siècles), Artefact 18 (2023) 117–137, https://doi.org/10.4000/artefact.13776.
[22] F. Zhang, The origin and development of traditional Chinese glazes and decorative ceramic colours, in: W.D. Kingery (Ed.), Technology to Modern Science, Ceramics and Civilization Series, 1, The American Ceramic Society, Colombus, 1985, pp. 163–180.
[23] W.D. Kingery, P.B. Vandiver, The Eighteenth-Century Change in Technology and Style from the Famille-Verte Palette to the Famille-Rose Palette, in: W.D. Kingery (Ed.), Technology and Style, Ceramics and Civilization Series, 2, The American Ceramic Society, Colombus, 1986, pp. 363–381.
[24] A. d'Albis, Traité de la Porcelaine de Sèvres, Faton, Dijon, 2003.
[25] M. Maggetti, A. d'Albis, Phase and compositional analysis of a Sèvres soft paste porcelain plate from 1781, with a review of early porcelain techniques, Eur. J. Mineral. 29 (3) (2017) 347–367, https://doi.org/10.1127/ejm/2017/0029-2627.
[26] P. Colomban, Glazes and Enamels, Chapter 10.6, in: P. Richet (Ed.), Encyclopedia of Glass Science, Technology, History, and Culture, 2, J. Wiley & Sons Inc., The American Ceramic Society, New York, 2021, pp. 1309–1325.
[27] E. Neri, C. Morvan, P. Colomban, M.F. Guerra, V. Prigent, Late Roman and Byzantine mosaic opaque "glass-ceramics" tesserae (5th-9th century), Ceram. Int. 42 (16) (2016) 18859–18869, https://doi.org/10.1016/j.ceramint.2016.09.033.
[28] B. Demirsar-Arli, G. Simsek Franci, S. Kaya, H. Arli, P. Colomban, Portable X-ray fluorescence (p-XRF) uncertainty estimation for glazed ceramic analysis: case of

Iznik tiles, Heritage 3 (4) (2020) 1302–1329, https://doi.org/10.3390/heritage3040072.
[29] P. Colomban, G. Simsek Franci, J. Burlot, X. Gallet, B. Zhao, J.-B. Clais, Non-invasive on-site pXRf analysis of coloring agents, marks and enamels of qing imperial and non-imperial porcelain, Ceramics 6 (1) (2023) 447–474, https://doi.org/10.3390/ceramics6010026.
[30] P. Colomban, G. Simsek Franci, M. Gironda, P. d'Abrigeon, A.-C. Schumacher, pXRF data evaluation methodology for on-site analysis of precious artifacts: cobalt used in the blue decoration of qing dynasty overglazed porcelain enameled at Customs District (Guangzhou), Jingdezhen and Zaobanchu (Beijing) Workshops, Heritage 5 (3) (2022) 1752–1778, https://doi.org/10.3390/heritage503009.
[31] P. Colomban, M. Gironda, G. Simsek Franci, P. d'Abrigeon, Distinguishing genuine imperial qing dynasty porcelain from ancient replicas by on-site non-invasive XRF and Raman spectroscopy, Materials 15 (16) (2022) 5747, https://doi.org/10.3390/ma15165747.
[32] K. Janssens, Modern Methods for Analysing Archaeological and Historical Glass, John Wiley & Sons, Chichester, 2013.
[33] L. Dussubieux, M. Golitko, B. Gratuze, Recent Advances in Laser Ablation ICP-MS for Archaeology, Springer, Heidelberg, Berlin, 2016.
[34] A.W. Miziolek, V. Palleschi, I. Schechter, Laser-induced Breakdown Spectroscopy (LIBS): Fundamentals and Applications, Cambridge University Press, Cambridge, 2006.
[35] P. Colomban, The on-site/remote Raman analysis with mobile instruments: a review of drawbacks and success in cultural heritage studies and other associated fields, J. Raman Spectrosc. 43 (11) (2012) 1529–1535, https://doi.org/10.1002/jrs.4042.
[36] H.G.M. Edwards, P. Vandenabeele, P. Colomban, Raman Spectroscopy in Cultural Heritage Preservation, Springer, Heidelberg, Berlin, 2023, https://doi.org/10.1007/978-3-031-14379-3.
[37] J. Castaing, M. Menu, Laboratory portrait: analysis of art works and nuclear physics at the Laboratory of Centre de Recherche et de Restauration des Musées de France, Nucl. Phys. News 16 (2006) 4–10, https://doi.org/10.1080/10506890601061437.
[38] I. Biron, S. Beauchoux, Ion beam analysis of Mosan enamels, Meas. Sci. Technol. 14 (2003) 1564–1578, https://doi.org/10.1088/0957-0233/14/9/308.
[39] R. Trittschak, M. Maggetti, A. d'Albis, G. Kozlowski, Analyse d'une assiette peinte par Jean-Jacques Pierre le Jeune à Sèvres en 1781, Keram. -Freund Schweiz 129 (2015) 50–62.
[40] P. Colomban, A.-T. Ngo, N. Fournery, Non-invasive Raman analysis of 18th century ChinesE Export/armorial Overglazed Porcelain: Identification of the Different Enameling Techniques, Heritage 5 (1) (2022) 233–259, https://doi.org/10.3390/heritage5010013.
[41] C. Helvaci, H. Mordogan, M. Cotaz, I. Gündogan, Presence and distribution of lithium in borate deposits and some recent lake waters of West-Central Turkey, Intern. Geol. Rev. 46 (2) (2004) 177–190, https://doi.org/10.2747/0020-6814.46.2.177.
[42] C. Helvaci, Borate deposits: an overview and future forecast with regard to mineral deposits, J. Boron 2 (2) (2017) 59. ⟨https://dergipark.org.tr/en/pub/boron/issue/31236/302668⟩.
[43] H. Tan, J. Su, P. Xu, T. Dong, H.I. Elenga, Enrichment mechanism of Li, B and K in the geothermal water and associated deposits from the Kawu area of the Tibetan plateau: constraints from geochemical experimental data, Appl. Geochem. 93 (2018) 60–68, https://doi.org/10.1016/j.apgeochem.2018.04.001.
[44] A.K. Hassan, L.M. Torell, L. Börjesson, H. Doweidar, Structural changes of B_2O_3 through the liquid-glass transition range: a Raman-scattering study, Phys. Rev. B 45 (22) (1992) 12797, https://doi.org/10.1103/PhysRevB.45.12797.
[45] R. Ciceo-Lucacel, I. Ardelean, FT-IR and Raman study of silver lead borate-based glasses, J. Non Cryst. Solids 353 (18–21) (2007) 2020–2024, https://doi.org/10.1016/j.jnoncrysol.2007.01.066.
[46] T. Satyanarayana, I.V. Kityk, M. Piasecki, P. Bragiel, M.G. Brik, Y. Gandhi, N. Veeraiah, Structural investigations on PbO–Sb_2O_3–B_2O_3:CoO glass ceramics by means of spectroscopic and dielectric studies, J. Phys. Condens. Matter 21 (24) (2009) 245104, https://doi.org/10.1088/0953-8984/21/24/245104.
[47] E. Moshkina, I. Gudim, V. Temerov, A. Krylov, Temperature-dependent absorption lines observation in Raman spectra of $SmFe_3(BO_3)_4$ ferroborate, J. Raman Spectrosc. 49 (10) (2018) 1732–1735, https://doi.org/10.1002/jrs.5430.
[48] C. Barboiu, B. Sala, S. Bec, S. Pavan, E. Petit, P. Colomban, J. Sanchez, S. de Perthuis, D. Hittner, Structural and mechanical characterizations of microporous silica–boron membranes for gas separation, J. Membr. Sci. 326 (2) (2009) 514–525, https://doi.org/10.1016/j.memsci.2008.10.052.
[49] P. Colomban, M. Maggetti, A. d'Albis, Non-invasive Raman identification of crystalline and glassy phases in a 1781 Sèvres Royal factory soft-paste porcelain plate, J. Eur. Ceram. Soc. 38 (2018) 5228–5233, https://doi.org/10.1016/j.jeurceramsoc.2018.07.001.
[50] P. Colomban, F. Ambrosi, A.T. Ngo, T.A. Lu, X.L. Feng, S. Chen, C.L. Choi, Comparative analysis of wucai chinese porcelains using mobile and fixed Raman microspectrometers, Ceram. Int. 43 (2017) 14244–14256, https://doi.org/10.1016/j.ceramint.2017.07.172.
[51] R. Kerr, N. Wood, Science and Civilization in China: Volume 5, Chemistry and Chemical Technology, Part 12, Ceramic Technology, Cambridge University Press, Cambridge, 2004.
[52] L. Pichon, B. Moignard, Q. Lemasson, C. Pacheco, P. Walter, Development of a multi-detector and a systematic imaging system on the AGLAE external beam, Nucl. Instrum. Methods Phys. Res. Sect. B Beam Interact. Mater. 318 (2014) 27–31, https://doi.org/10.1016/j.nimb.2013.06.065.
[53] L. Pichon, T. Calligaro, Q. Lemasson, B. Moignard, C. Pacheco, Programs for visualization, handling and quantification of PIXE maps at the AGLAE facility, Nucl. Instrum. Methods Phys. Res. Sect. B Beam Interact. Mater. 363 (2015) 48–54, https://doi.org/10.1016/j.nimb.2015.08.086.
[54] J.A. Maxwell, W.J. Teesdale, J.L. Campbell, The Guelph PIXE software package II, Nucl. Instrum. Methods Phys. Res. Sect. B Beam Interact. Mater. 95 (3) (1995) 407–421, https://doi.org/10.1016/0168-583X(94)00540-0.
[55] K. Govindaraju, Report (1980) on three GIT-IWG rock reference samples: anorthosite from Greenland, AN-G; Basalte d'Essey-la-Côte, BE-N; Granite de Beauvoir, MA-N, Geostand. Newsl. 4 (1) (1980) 49–138, https://doi.org/10.1111/j.1751-908X.1980.tb00274.x.
[56] K. Govindaraju, I. Roelandts, Second report (1993) on the first three GIT-IWG rock reference samples: anorthosite from Greenland, AN-G; Basalte d'Essey-la-Côte, BE-N; Granite de Beauvoir, MA-N, Geostand. Newsl. 17(2) 227–294. ⟨https://doi.org/10.1111/j.1751-908X.1993.tb00142.x⟩.
[57] E.P. Vicenzi, S. Eggins, A. Logan, R. Wysoczanski, Microbeam characterization of Corning archeological reference glasses: New additions to the Smithsonian Microbeam Standard collection, J. Res. Natl. Inst. Stand. Technol. 107 (2002) 719, https://doi.org/10.6028/jres.107.058.
[58] Bruker Nano GmbH, Information Depth. ⟨https://xrfcheck.bruker.com/InfoDepth⟩ (Accessed 6 December 2023). (2023).
[59] P. Colomban, B. Kırmızı, G. Simsek Franci, Cobalt and associated impurities in blue (and green) glass, glaze and enamel: relationships between raw materials, processing, composition, phases and international trade, Minerals 11 (2021) 633, https://doi.org/10.3390/min11060633.
[60] E.M. Levin, C.R. Robbins, H.F. McMurdie, Phase Diagrams for Ceramists, Vols I-IV, 1964,1969,1975, The American Ceramic Society, Westerville, 1981.
[61] J. Van Pevenage, D. Lauwers, D. Herremans, E. Verhaeven, B. Vekemans, W. De Clercq, L. Vincze, L. Moens, P. Vandenabeele, A combined spectroscopic study on chinese porcelain containing Ruan-Cai colours, Anal. Methods 6 (2014) 387–394, https://doi.org/10.1039/C3AY41072B.
[62] R. Giannini, I.C. Freestone, A.J. Shortland, European cobalt sources identified in the production of Chinese famille rose porcelain, J. Archaeol. Sci. 80 (2017) 27–36, https://doi.org/10.1016/j.jas.2017.01.011.
[63] D.E. Norris, D. Braekmans, K. Domoney, A.J. Shortland, The composition and technology of polychrome enamels on Chinese ruby-backed plates identified through nondestructive micro-X-ray fluorescence, X-ray Spectrom. 49 (2020) 502–510, https://doi.org/10.1002/xrs.3144.
[64] D.E. Norris, D. Braekmans, A.J. Shortland, Technological connections in the development of 18th and 19th century Chinese painted enamel, J. Archaeol. Sci. Rep. 42 (2022) 103406, https://doi.org/10.1016/j.jasrep.2022.103406.
[65] D.E. Norris, D. Braekmans, A.J. Shortland, Emulation and technological adaptation in late 18th century cloisonné-style Chinese painted enamel, Archaeometry 64 (4) (2022) 951–968, https://doi.org/10.1111/arcm.12757.
[66] H.W. Liu, H. Wang, P.Q. Duan, H. Gao, R. Zhang, L. Qu, The Qianlong Emperor's order: scientific analysis helpsfind French painted enamel among Palace Museum collections, Herit. Sci. 10 (2022) 132, https://doi.org/10.1186/s40494-022-00764-9.